Eur. Phys. J. B **40**, 489–497 (2004)
DOI: 10.1140/epjb/e2004-00163-4

THE EUROPEAN PHYSICAL JOURNAL B

# Arrays of Ni nanowires in alumina membranes: magnetic properties and spatial ordering

M. Vázquez[1,a], M. Hernández-Vélez[1], K. Pirota[1], A. Asenjo[1], D. Navas[1], J. Velázquez[2], P. Vargas[3], and C. Ramos[4]

[1] Instituto de Ciencia de Materiales, CSIC, 28049 Madrid, Spain
[2] CAI XRD, Fac. Químicas-UCM, 28040 Madrid, Spain
[3] Dept. Física, Univ. Técnica F. Sta. M[a], Valparaiso, Chile
[4] Instituto Balseiro, Centro Atómico, 8400 Bariloche, Argentina

Received 24 November 2003
Published online 15 June 2004 – 

**Abstract.** Magnetic characteristics of arrays of Ni nanowires embedded in porous alumina are reviewed as a function of their spatial ordering. The different steps for the controlled production of highly-ordered nanowires is firstly described. Nanopores are formed into an hexagonal symmetry arrangement by self-organized process during anodization of pure Al. Parameters of the anodization allow us to control their diameter, hexagonal lattice parameter and size of crystalline domains. Subsequently, Ni nanowires are grown inside the pores by electrodeposition. Control of the pores filling and of geometrical ordering characteristics has been performed by SEM, HRSEM, RBS and AFM techniques. The magnetic characterisation of the arrays has been achieved by SQUID and VSM magnetometers, while information on the magnetic state of individual nanowires is obtained by MFM. Experimental studies are presented, particularly coercivity and remanence, for arrays with different degree of ordering (crystalline domains up to around 1 $\mu$m), and for ratio diameter to lattice parameter (diameter ranging between 20 and 180 nm, and distance between 35 and 500 nm). FMR studies have allows us to obtain complementary information of the anisotropy and magnetic characteristics. A modelling of multipolar interacting nanowires is introduced to account for the influence of short and long range ordering degree of the arrays.

**PACS.** 75.60.Jk Magnetization reversal mechanisms – 81.15.Pq Electrodeposition, electroplating

## 1 Introduction

Studies on various kinds of highly-ordered arrays of nanowires is nowadays attracting growing interest [1]. This is firstly a consequence of the development of experimental techniques to fabricate such arrays in a controllable way [2,3]. The high ordering, together with the intrinsic nature of nanowires may give rise to outstanding cooperative properties of fundamental and technological interest in a broad range of topical areas as semiconductors, magneto-optics, biomedicals, miniaturized sensors or magnetic storing [4–6]. The understanding of the behavior of such arrays, different from bulk and even from film systems, is thus of importance from both theoretical and practical points of view.

Patterning nanomagnetic elements 10 to 100 nm in size is being currently achieved by different methods: electron-beam, X-ray or imprint lithography techniques [2,7,8]. This offers in principle the potential interest of increasing the areal density in magnetic recording media up to around 300 Gbit/in$^2$ in arrays of magnetic nanoelements with about 50 nm periode distance, assuming each nanomagnet or a very reduced number of them represents one single bit of information. Alternative techniques include the use of nanoporous membranes fabricated by irradiation with heavy ions and by chemical etching of polymers [9,10] or mica [11], and by self-assembling methods [12,13] which are employed as templates for nanowire elements. In all cases, combined electrodeposition techniques are subsequently used to fill the membranes nanopores. Nanowires arrays in polymer membranes are spatially randomly distributed, while a higher geometrical symmetry ordering can be achieved in alumina membranes. Here, the self-organization process of the nanopores during their formation induces a dense packing of nanowires. Thickness of membranes and accordingly length of nanowires vary within the range of few $\mu$m. The size of these templates, with typical cross-section in the range of a few cm$^2$, make them nearly ideal systems to study fundamental problems in micromagnetism because of the high degree of nanowires spatial ordering (with hexagonal symmetry) that can extend along several microns without perturbance. The diameter of nanowires can be controlled and the whole array can

[a] e-mail: mvazquez@icmm.csic.es

be approached to a regular lattice of parallel nanowires. These nanowires provide certainly a less-expensive, versatile and reproducible systems to investigate magnetization processes and transport phenomena.

From a geometrical point of view, an important achievement is the controlled production of the densely-packed highly-ordered nanowires arrays. Magnetically, additional requirements are that each nanowire exhibit a longitudinal magnetization easy axis and that its anisotropy be strong enough to reduce the effect of stray fields perturbance of neighboring nanowires. That is important not only because of the possibilities to employ the arrays in storage or sensor devices but also for micromagnetics and other fundamental studies.

Research on magnetic behavior has been reported previously on arrays of nanowires prepared by electrodeposition techniques on polycarbonate [14] and alumina templates [15–17]. These studies are dealing on arrays of most characteristic magnetic elements as Fe, Ni and Co, but also on alloyed [18,19] or layered nanowires [20], and concern the magnetization reversal process of nanowires and their magnetic interactions. Other aspects of interest include magnetotransport phenomena [21,22] that will not be considered here. While shape mostly determines the magnetization easy axis in Fe and Ni [21,23], in the case of Co nanowires magnetocrystalline anisotropy with nearly transverse easy axis balances the shape anisotropy [24] so that, Co is not a suitable element. Attempts have been also done to increase magnetic hardness using CoPt or FePt alloys and various thermal processing [25].

Investigations on the magnetization reversal of nanowires have been performed by experimental techniques [26,27] and micromagnetics modelling [28]. Individual nanowires are taken as a first approximation to be single-domain with axial magnetization. Magnetization reversal of wires with diameter in the range of few micrometers takes place by nucleation of domain walls at the ends where magnetization reversal starts and by subsequent depinning and propagation along the entire wire [29]. Each wire contributes with a small square hysteresis loop displaced accordingly to the stray field of the neighbouring wires. For nanowires with diameter in the range of around 50 to 400 nm, a curling rotational model has been proposed combined with a nucleation-propagation process. The wire diameter, $\phi$, is larger than the wall thickness (or actually the exchange correlation length), $\phi_w$, which in the case of Fe, Co and Ni lies within the range of 10 to 50 nm. For the so-called 1-D magnetic wire systems, $\phi < \lambda_w = 2\ (A/K)^{1/2}$ ($A$ being the exchange constant and $K$ the longitudinal anisotropy constant) magnetization should reverse at unison by coherent rotation. Nevertheless, although nearly non-dependent on wire diameter, switching field takes values smaller than expected when measuring at the very low temperature range that suggests the existence of some alternative mechanism involving the formation of a kind of small domain wall at the end or at local non-homogeneities, and its subsequent propagation [30–33]. The determination of actual closure structures at the ends seems then to be rather important to deepen into the knowledge of the reversal process.

Ferromagnetic resonance studies on arrays of magnetic nanowires has been proved to supply additional information other than magnetometry techniques. Only a few works have been published about the topic mainly in polycarbonate membranes [34,35], considering for example the influence of the array porosity, the distributed effective anisotropy field and the angular spread or misorientaion of nanowires.

The objective of the present work has been to summarize the results of our investigations on arrays of Ni nanowires. The steps for the production of nanoporous membranes as templates for the nanowires are described in the next section together with the techniques employed to determine their spatial arrangement. Then, magnetic properties are collected for arrays with different geometrical characteristics as nanowire diameter, interwire distance or lattice parameter of the hexagonal symmetry array, and degree of the ordering in the array. General information is gained by magnetometer techniques while more local details are obtained by MFM. FMR measurements are also shown to give noticeable information. Finally, the magnetostatic interactions among nanowires are modelled. It is shown that multipolar rather than dipolar interactions must be considered to account for the experimental results.

## 2 Structural characterization of unfilled and Ni filled nanoporous alumina membranes

To fabricate the nanoporous alumina membrane with highest quality and controlled geometrical characteristics one has to take careful procedures. Nanoporous alumina membranes with hexagonal ordering have been prepared by a two-step anodization process [12]. Aluminum foils with high purity (99.999%) have been used as starting material. Before being placed inside an anodization cell, foils are firstly degreased and electropolished. Anodization processes at controlled temperature are done inside the anodization cell using oxalic, sulfuric or phosphoric acid solutions. Nanopores form by self-assembling process, and parameters of first anodization determine important characteristics of final arrays as ordering degree of final pores arrays (e.g., size of crystalline domains with hexagonal symmetry) and interpore distance (60 nm to 500 nm). The porous alumina is then removed, and a second anodization is performed. Afterwards, the thickness of the alumina barrier layer is reduced while the diameter of the nanopores are finer controlled. Nanowires diameter has been controlled between 18 and 35 nm for interwire distance of 65 nm employing sulphuric acid as electrolthical bath, and between 30 and 85 nm diameter for interwire distance of 105 nm with oxalic acid as bath. Employing phosphoric acid allows one to obtain 180 nm diameter nanowires separated 500 nm. The length of the nanopores, and consequently of the nanowires, is typically in the range from 500 to 5000 nm. Results presented here correspond to nanopores 4000 nm long.

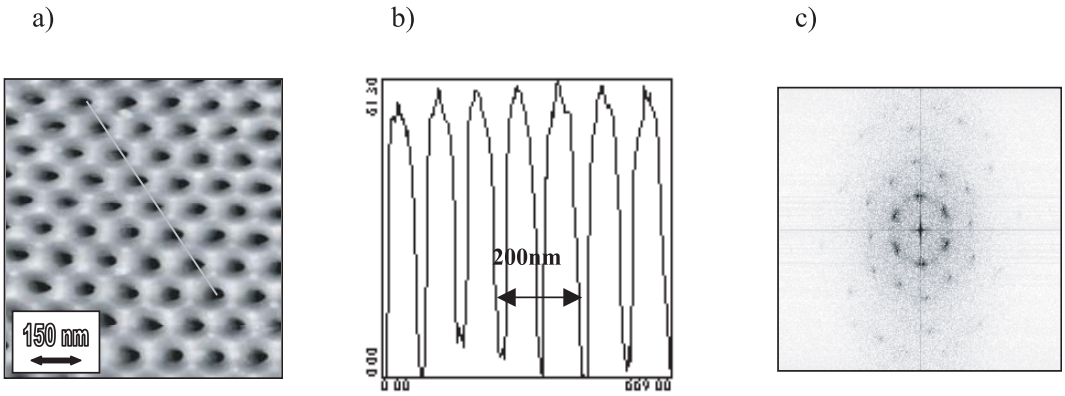


**Fig. 1.** The quality of the hexagonal array of a nanoporous membrane can be observed by an AFM image (a) a profile of the sample (b), and FFT analysis clearly showing which the existence of long range ordering of hexagonal symmetry.

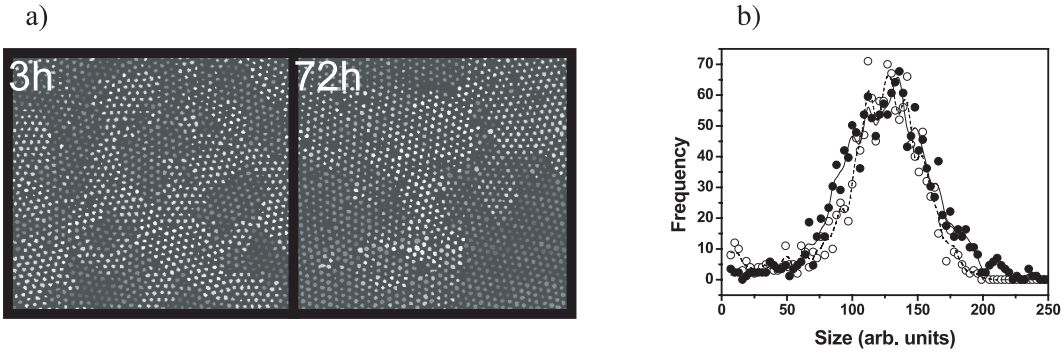


**Fig. 2.** SEM images corresponding to two hexagonal arrays of Ni nanowires with different 2D-polycrystalline arrangement as originated by different time of first anodization (3 h and 72 h) (a). Histograms showing the size and the standard distribution of nanowires cross-section for the arrays in (a) [(○) and (●) are for the samples with 3 h and 72 h first anodization times, respectively] (b).

Nanopores are filled by electrodeposition of magnetic metals through constant current pulses, constant voltage pulses, current-voltage mixture pulses [36], and by alternating pulses [37]. In our case, we have used the alternating pulse techniques since it allows us an enhanced filling degree of nanopores. The quality of the final ordering of the nanoporous membranes can be observed in Figures 1a, 1b and 1c that respectively show an AFM image, the profile along a direction of hexagonal symmetry, and the Fast Fourier Transform. Particular studies in local regions have allowed us to identify local defects in the arrays (actually, the lack of individual pores originates domains rotated with respect to previous one) giving rise to the polycrystalline character of the long range arrangements.

Particularly, the time of first anodization process is proved to be an important parameter to determine the final size of such domains. We have performed a study at increasing the time of first anodization: 3, 18, 24 and 72 h. The SEM images shown in Figure 2a show the results after 3 and 72 h first anodization time (second anodization time is 2 h in both cases). Diameter of nanopores is 35 nm and interpore distance 105 nm. Figure 2b shows the histograms for the size and standard distribution of nanowires cross-sections of arrays in Figure 2a. It is important to emphasize that slightly larger average nanopore diameter (10%) and standard deviation (6%) are observed for the arrays obtained for the longest time of first anodization. Alternatively, it suggests that although long time of first anodization induces long range ordering, a short time of first anodization results in a higher homogeneity in the nanopores cross-section.

Final steps include the control of filling of nanopores by Rutherford Back-Scattering technique, RBS, (local Ni surface overflow observed in Figure 3a arises from inhomogeneous growing rate at different nanopores [38]), and subsequent polishing of the membrane surface. Figure 3b shows a HRSEM image of a long range ordered array. Further details about preparation can be found elsewhere [39].

## 3 Magnetizatic behavior of Ni nanowires arrays

### 3.1 Magnetic anisotropy, hysteresis loops and magnetic interactions

The magnetic behavior of the nanowires arrays has been first determined by SQUID and VSM magnetometers. This type of measurements allows us the determination of magnetic parameters of the arrays as remanence, coercivity or field to reach saturation. All these parameters are

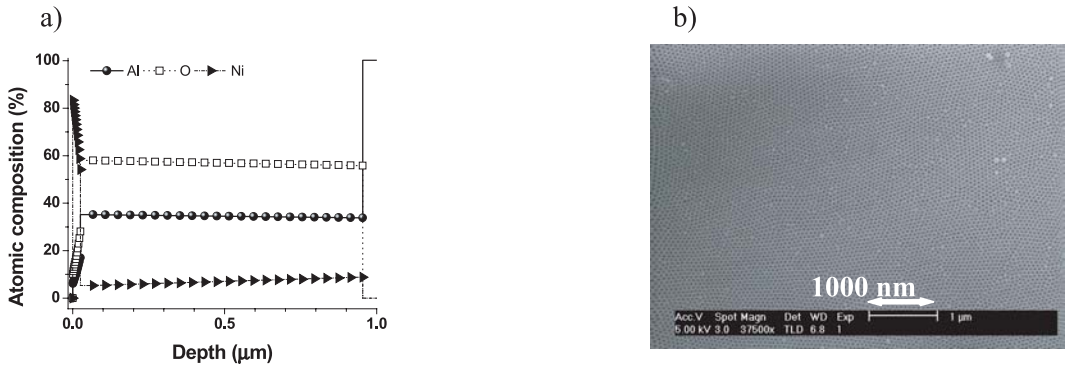


**Fig. 3.** Atomic percentage of elements present in the alumina membrane after filling of nanopores with Ni. Complete filling of pores and Ni overflow is detected by RBS technique (a). HRSEM image of an array (note that average size of domains is larger than around 1 $\mu$m) (b).

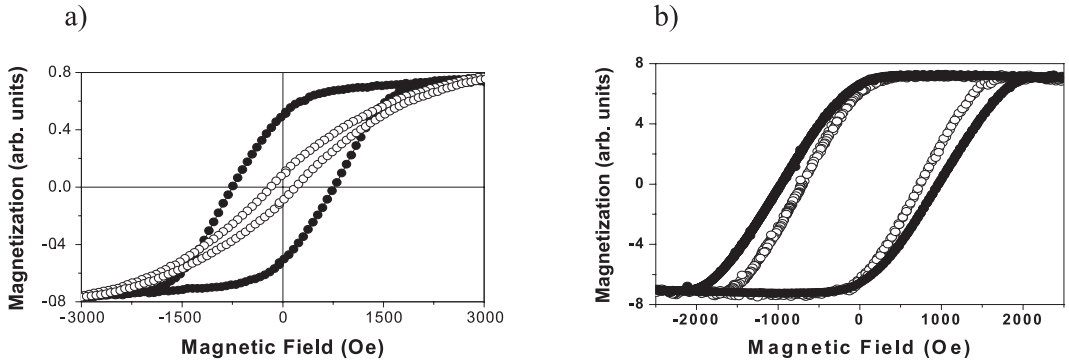


**Fig. 4.** Hysteresis loops of a Ni filled alumina membrane (35 nm diameter and 105 nm interwire distance after 24 h first anodization followed by 2 h second anodization time) measured with applied field parallel to the nanowire axis (•) and in-plane of the membrane (perpendicular to the wires axis) (○) (a). Hysteresis loops for the arrays shown in Figure 2a (b).

also connected with the magnetostatic interactions among nanowires. Firstly, the existence of an effective longitudinal magnetic anisotropy (parallel to the nanowires axis) is checked by measuring the longitudinal and transverse (in-plane of the membrane) hysteresis loops as can be observed in Figure 4a. In that particular case (Ni nanowires 35 nm in diameter, separated 105 nm), an effective axial magnetic anisotropy can be deduced with anisotropy field of around 2.5 kOe. In fact, the effective magnetostatic field, $H_{eff}$, should decrease linearly with increasing the filling factor and finally change from axial to transverse easy axes.

It is noticeable that arrays with different size of polycrystalline domains of hexagonal symmetry show also different magnetic behavior. Figure 4b shows the hysteresis loops corresponding to the arrays of nanowires shown in Figure 2a. Coercivity takes a larger value, (960 Oe in comparison with 720 Oe), as well as remanence. These changes have been correlated with the magnetic interactions among nanowires [40].

The ratio nanowire diameter to interwire distance, $r = d/D$, is an important parameter to determine the parameters of the loops as coercivity or remanence. Figure 5a shows the hysteresis loops for wires ranging in diameter between 30 and 80 nm being separated 105 nm. Figure 5b in turn shows that coercivity and remanence decrease with increasing the ratio $r$. Results are also included for nanowires separated 65 nm ranging in diameter between 20 and 30 nm. The observed decrease should be probably related to an enhanced magnetostatic interaction between the densely packed nanowires.

While hysteresis loops measured by SQUID or VSM magnetometers allows us to obtain information on the array as a whole, magnetic force microscopy, MFM, is useful to inform us of the magnetic state of individual nanowires. Figure 6a shows the MFM image of a particular array in a remanence state after magnetic saturation, while in Figure 6b (at a localized region) it is possible to identify nanowires magnetized up or down according to the image contrast. What is important also to mention is that in some nanowires intermediate contrast is observed denoting the presence of particular closure structures at the very end of nanowires.

### 3.2 Dynamic processes: FMR measurements

FMR studies supplies information about fundamental magnetic magnitudes as spontaneous magnetization, spin-waves or gyromagnetic factor, but also as we are interested in the present case, on the magnetic anisotropy [41,42]. The total anisotropy field of our system would contain magnetocrystalline, magnetoelastic and shape

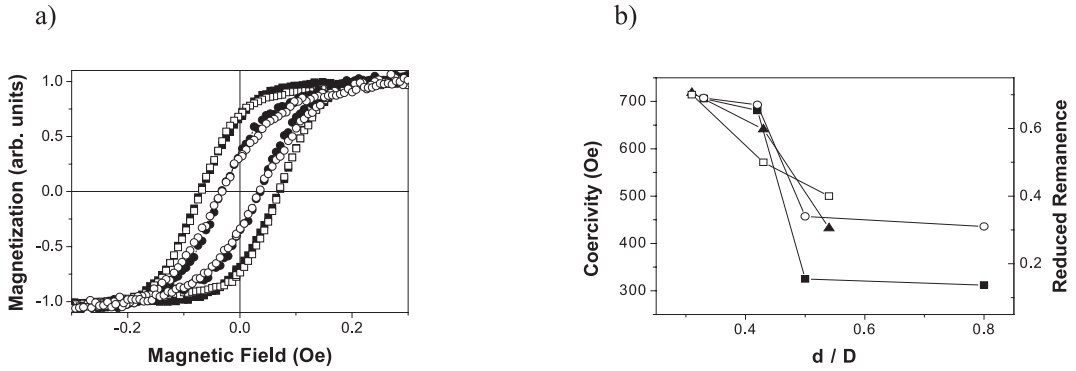


**Fig. 5.** Hysteresis loops as a function of the nanowire diameter for Ni nanowires separated 105 nm having diameters of 35 nm (■), 44 nm (❑), 53 nm (●) and 83 nm (○) (a). (b) Dependence of coercivity [membranes prepared in oxalic (■) and sulphuric (▲) acids] and reduced remanence [oxalic (○) and sulfuric membranes (❑)] as a function of the ratio diameter to interwires distance $d/D$.

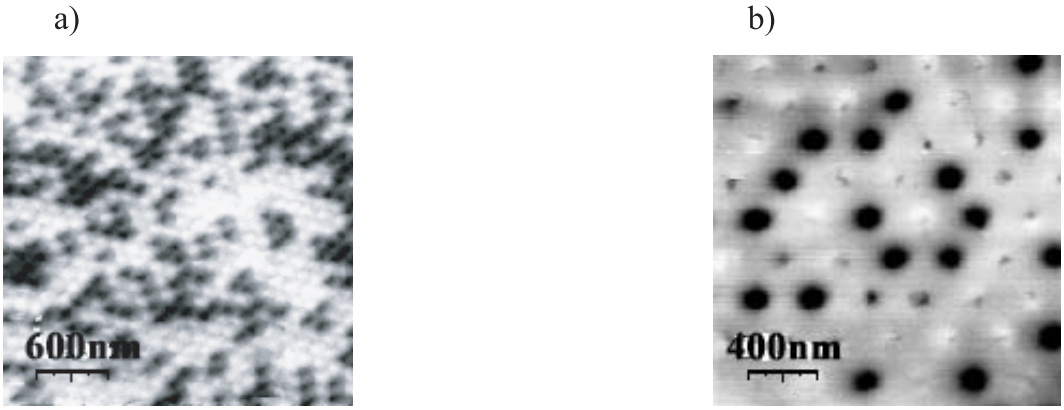


**Fig. 6.** MFM image in a remanent state (a). Identification of magnetic state of individual nanowires can be determined (b).

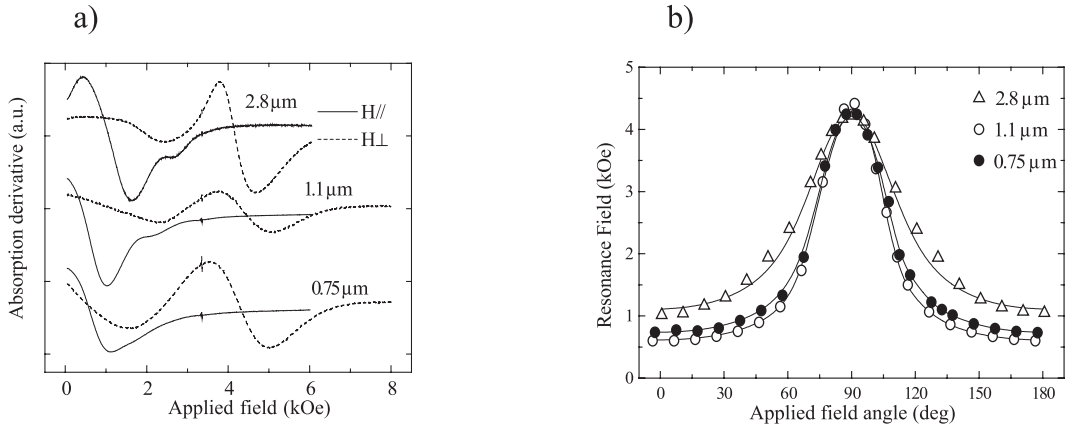


**Fig. 7.** FMR signal at 9.4 GHz for applied field parallel, $H_{//}$, and perpendicular, $H_{\perp}$, to the nanowires axis for arrays with different ordering degree. Spectra were shifted for clarity (a). Observed angular variation of the FMR signal and best fits (full lines) using equation (4) (b).

contributions and can be expressed as:

$$H_{anis} = H_{cr} + H_{\sigma} + H_{sh}. \quad (1)$$

Nevertheless, due to the special characteristics of the array, most important contribution is that one coming from the shape [34]:

$$H_{sh} = 2\pi Ms(1 - 6f) \quad (2)$$

where the filling factor given by $f = 3.67(d/D)^2$ determines how the effective shape anisotropy magnetization easy axis goes from axial to in-plane directions.

FMR measurements presented here have been performed in a Bruker EMX300 spectrometer at 9.4 GHz. Figure 7a shows the FMR spectra of three Ni nanowire arrays having 35 nm diameter and 105 nm interwire distance (mean values) [43] characterized by a different

polycrystalline ordering degree. Results are for applied fields parallel and perpendicular to nanowires axis. As observed, for example in the case of parallel field spectra, the width of the absorption line is about 1 kOe and a kind of shoulder at around 1 kOe above the resonance is observed specially for the sample showing the highest ordering degree.

In order to get additional information, the angular dependence of the resonance field, $H_r$, has been further studied. The equilibrium state considering a rotational magnetization process is given by:

$$H_r \sin\phi = H_{anis} \sin 2(\phi - \phi_\alpha) \tag{3}$$

where $H_r$ is the resonance field, $H_a$ is the effective anisotropy field, $\varphi$ is the equilibrium angle between the applied field and the magnetization, and $\varphi_a$ is the angle between the field and the anisotropy axis (along the wire axis). The resonance condition for uniaxial anisotropy can be taken as [31]:

$$(\omega/\gamma)^2 = [H_r \cos\varphi + H_a \cos^2(\varphi - \varphi_a)][H_r \cos\varphi + H_a \cos 2(\varphi - \varphi_a)]. \tag{4}$$

Figure 7b shows the experimental angular variation observed and the best fit to equation (4). The parameters obtained from the fittings are: $H_a = 1.99$, 2.32, and 2.21 kOe for the arrays showing higher, intermediate and lower ordering, respectively. While the value of the anisotropy field for an isolated Ni nanowire is 3.05 kOe, larger than that deduced in our case but still smaller than that reported in [35]. The main difference with [35] is the density of nanowires in the array, which in our case is estimated to give a filling factor $f = 0.10$ from structural information and geometrical consideration. This leads to $H_a = 2.15$ kOe in good agreement with the observed values.

Alternatively, the difference between the anisotropy field expected for a wire and that measured experimentally can be employed to determine the filling factor. From an analysis of that difference it is possible to deduce that the array with formally the higher ordering presents nevertheless larger diameter by around 10% compared with that of the less ordered array. That is in agreement with what was deduced in a previous section by analyzing the SEM images.

On the other hand, FMR studies on the line width at given band allows us quantitative analysis on the distribution of parameters of individual wires. The width of the absorption signal can be expressed as:

$$\Delta H_\rho = \Delta H_{\Delta\alpha} + \Delta H_{int} \tag{5}$$

where the two terms arise from the fluctuations in anisotropy and intrinsic contributions respectively. Further studies are needed to interpret experimental line width of around 0.3 kOe since neither crystalline nor shape anisotropies contributions can be claimed. Finally, the shoulder observed in the spectra specially for that one with highest ordering at around 1 kOe above the resonance should be probably related to slightly different filling factors or to the different ordering degree. Also, exchange/dipole spin-wave modes could be suggested.

## 4 Modelling of magnetic interactions: influence of spatial ordering

As mentioned before, a dense packing of nanowires is of interest to achieve higher density of information. But a higher packing leads in parallel to enhance the magnetostatic interactions among nanowires. In fact, as has been mentioned in a previous section, it increases the filling factor and finally, the interaction results in a shearing of the hysteresis loops which is equivalent to the inclination of the easy magnetization direction from the axis of the nanowires to the plane of the membrane. Each isolated nanowire is assumed to consist of a single domain structure because of the large uniaxial anisotropy along its axis mainly due to the strong shape anisotropy. Only some closure structures or deviations of magnetization from axial to circumferential direction are considered to appear at the ends in order to reduce the stray fields energy of the poles densities. So that, as a first approximation nanowires have been first considered as magnetic dipoles, and the problem has been treated as interactions among many dipoles [44]. The dipoles being located at positions following the hexagonal symmetry. Additionally, the magnetostatic interaction of nanowires in the array gives rise to self-organized collective magnetization that can be ascribed to complex systems described by fractals [45].

We have followed two techniques to model the magnetic interactions between nanowires. The first one was introduced for the case of interacting bistable magnetic microwires [46], where the following system of equations is solved iteratively:

$$M_i = M_i(H_i) = M_i \left( H_{ap} - \sum_{j=1}^{j=N} K_{ij} M_j \right) \tag{6}$$

being $N$ the number of wires, $M_i$ the magnetization of $i$th wire, $H_i$ the effective magnetic field acting on the $i$th wire, that is, the axial applied magnetic field, $H_{ap}$, and the sum of axial fields generated by each $j$th neighbouring nanowire acting on the $i$th nanowire, $K_{ij}M_j$. Coefficients $K_{ij}$ are determined solving Laplace's equation for a homogeneously axially magnetized wire as $K_{ij} = -(1/M_j)[\partial V_j(r,z)/\partial z]$, being $V_j$ the magnetic potential created by $j$th nanowire [47]. It shows that although under some conditions dipolar approach can be used, for the case of densely packed nanowires a multipolar approach is required. Think of a typical case where diameter of nanowires and interwire distance are of the same order (let us say 50 nm and 100 nm respectively), while the length of the wires are around 1 $\mu$m.

Alternatively, Monte Carlo simulations have been also performed. Here the equilibrium is determined considering

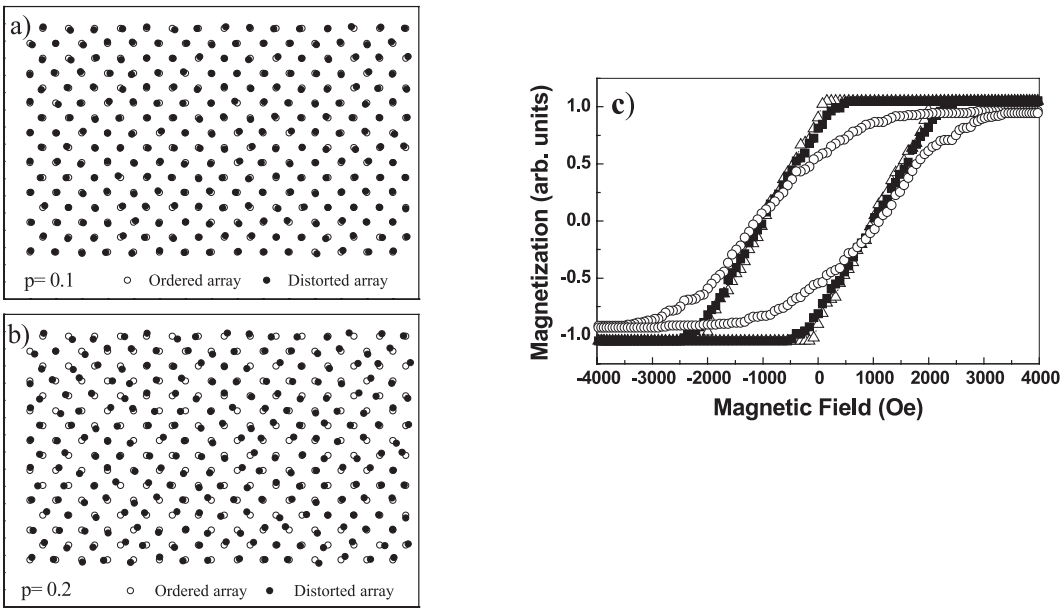


**Fig. 8.** Modeling disorder on nanowires arrays with hexagonal symmetry. Full dots denote ideally ordered hexagonal array, whereas open circles correspond to disordered arrays assuming $\delta = 0.1$ (a) and $\delta = 0.2$ (b) distortion as defined in the text. Influence of disorder on the hysteresis loops of hexagonal arrays of nanowires using the iterative model [$p = 0$ ($\triangle$), $p = 0.2$ (■), and $p = 0.5$ ($\circ$)] (c).

the total energy given by the sum of Zeeman, dipole-dipole interaction and anisotropy energy terms:

$$E = -\sum_j \vec{m}_j \cdot \vec{H}_{ap} - \sum_{i>j} \frac{\vec{m}_i \cdot \vec{m}_j - 3\left(\vec{m}_i \cdot \hat{n}_{ij}\right)\left(\vec{m}_j \cdot \hat{n}_{ij}\right)}{r_{ij}^3} - \sum_j k_j \left(\frac{\vec{m}_j}{m_j} \cdot \hat{z}\right)^2 \quad (7)$$

$r_{ij}$ being the distance between the magnets at sites $i$ and $j$, and $n_{ij}$ is the unitary vector going from magnet $i$ to magnet $j$. Anisotropy within each nanowire is characterized by a strength $k_j$ on the magnet at the $j$th site, and the axial applied magnetic field, $H_{ap}$, driving the hysteresis curve is superimposed to previous internal interactions. The underlying hexagonal lattice enters only in the dipolar contribution to the energy through the interwires distances $r_{ij}$. The anisotropy strength, $k_j$, is first assumed to be the same for all sites of the lattice, and its value must be introduced together with the magnetic moment of individual wires for the simulations.

The influence of the ordering degree has been studied in [40], where a distortion of the hexagonal arrangement was introduced in order to simulate the different ordering degree of the arrays (see for example Fig. 2a). Disordered arrays are generated by deviations from the hexagonal array in the following way: coordinates of each nanowire are set to $(x_0 + p\alpha,\ y_0 + p\alpha)$, where $(x_0,\ y_0)$ are the coordinates for the ideally ordered hexagonal array, $p$ is a "degree of disorder" parameter and $\alpha$ is a random variable homogeneously distributed in the range $-1 < \alpha < +1$. The parameter $p$ measures then the array disorder, and it ranges from 0 up to the lattice parameter, $\Delta$ (for example, $p = 0.2$ denotes that interwire distance can be locally enlarged or reduced up to $1.2\Delta$ and down to $0.8\Delta$, respectively). Figure 8a shows two randomly generated distributed arrays for the cases of $p = 0.1$ and 0.2. Figure 8b shows the hysteresis loops corresponding to fully ordered, and two disordered lattices. As observed, disorder results in a magnetic hardening: an increase of the field required to reach magnetic saturation and a reduced remanence as a consequence of the stronger interaction of closest wires. Coercivity remains otherwise almost unchanged.

Modeling allows us to introduce distributed values of anisotropy field for individual nanowires or even for the effective magnetization creating the stray fields. Figure 9a shows the modeled loops for two anisotropy fields of 1.0 and 1.3 kOe. Now, an increase of anisotropy field induces enhancement of coercivity, remanence and field to reach saturation. A compromise is observed in Figure 9b, where higher ordering degree with smaller anisotropy is compared with disordered array but with larger anisotropy. It is to be noticed that loops in Figure 9b fit really well with the experimentally observed (see Fig. 4b). It appears thus that high-ordered arrays behave as if characterized by a smaller anisotropy field. In fact, that seems to correlate with the differences in short range and long range ordering experimentally deduced (see Fig. 2b): the averaged area of the nanowire faces in the 72 h sample is 6% larger with respect to the 3 h sample, moreover the standard deviation is also 10% larger. It indicates that actually nanowires in the 72 h anodization time array behaves as more disordered at the local scale although showing larger domains size at higher long range scale. The observed fluctuations of the diameter and of the shape of the cross-section of nanowires should result in an

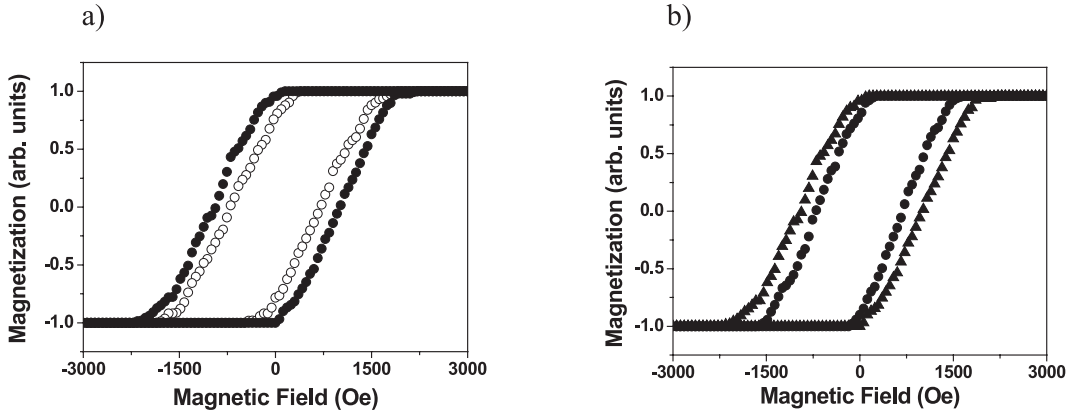


**Fig. 9.** Modeled Monte Carlo axial hysteresis loops. On hexagonal ordered and disordered lattices. Magnetization curves are for 1.0 (○) and 1.3 (●) kOe anisotropy field of individual nanowires (a). Loops corresponding to ordered array with larger anisotropy field (●) in comparison to disordered array with smaller anisotropy (▲) (b).

increasing local disorder but with individually larger coercivity for the array with longer anodization time which on the other hand would show higher ordering at larger geometrical scale.

The magnetostatic interaction in the hexagonal array of nanowires, and therefore, the distribution of the direction of individual magnetizations, can be additionally analyzed by considering an equivalent system: a set of disks magnetically charged arranged with hexagonal symmetry. Due to the large ratio length to diameter in nanowires, the interaction is stronger between the ends of the neighboring nanowires than between charges at opposite ends of the same nanowire. By calculating the magnetostatic energy of the system through the magnetic potential of the set of disks, the equilibrium configuration can be obtained, being very similar to that experimentally shown in Figure 6b that can be explained as a consequence of the distribution of individual magnetizations and the strength of the magnetostatic interaction.

## 5 Final remarks and conclusions

In the present manuscript we have collected information on various viewpoints regarding the synthesis and characterization of Ni nanowires arrays in porous membranes, on the magnetic behavior characterized by various techniques, and the simulation of that behavior in particular cases.

It has to be mentioned first that long range order of hexagonal symmetry can be controlled by the parameters of first anodization. The longer the anodization time the larger the size of ordered regions with average size up to a few $\mu$m. The diameter of nanowires is controlled in a subsequent step. It is to be noticed that complete filling of nanopores can be checked by RBS technique.

Concerning parameters of the hysteresis loops as coercivity and remanence, it is shown that ratio diameter of nanowires to distance between them is very important to determine their values. In fact, both parameters decrease with increasing that ratio as a consequence of the strengthening of the magnetostatic interaction.

Measurements of FMR have allowed us to confirm (as done with detailed analysis from SEM images) that arrays with higher ordering present larger non-homogeneity in the diameter of the wires.

Simulation of hysteresis loops by Monte Carlo and iterative techniques have been developed to interpret the dependence of hysteresis loops with the ordering degree.

Finally, it should be mentioned that controlled fabrication of these types of nanowire arrays can be exploited in a number of fundamental and applied research involving multidisciplinary techniques.

The authors wish to thank the important contribution to this work of Prof. Gösele, Dr. K. Nielsch, Dr. F. Paszti, Dr. V. de la Prida, R. Sanz and D. Laroze. The work has been supported by the Autonomous Community of Madrid under project CAM 07N/0086/2002.

## References

1. D. Appell, Nature **419**, 553 (2002)
2. J.I. Martín, J. Nogués, K. Liu, J.L. Vicent, I.K. Schuller, J. Magn. Magn. Mater. **256**, 449 (2003)
3. C. Ross, Ann. Rev. Mater. Res. **31**, 203 (2001)
4. See J. Magn. Magn. Mater. 249 (2002) Vols. 1–2 devoted to the *Proceedings of the Int. Workshop on Magnetic Wires, San Sebastián, Spain*
5. R. O'Barr, S.Y. Yamamoto, S. Schultz, W. Xu, A. Scherer, J. Appl. Phys. **81**, 4730 (1997)
6. R. Skomski, H. Zeng, M. Zheng, D.J. Sellmyer, Phys. Rev. B **62**, 3900 (2000)
7. C. Ross et al., J. Vac. Sci. Techn. B **17**, 3168 (1999)
8. R. O'Barr, R.M. Lederman, S. Schultz, W. Xu, A. Scherer, R. J. Tonicci, J. Appl. Phys. **79**, 5303 (1996)
9. T.M. Witney, J.S. Jiang, P. Searson, C. Chien, Science **261**, 1316 (1993)
10. L. Piraux, J.M. George, J.F. Despres, C. Leroy, E. Ferain, R. Legras, K. Ounadjela, A. Fert, Appl. Phys. Lett. **65**, 2484 (1994)
11. C.L. Chien et al., in reference [12], p. 146
12. H. Masuda, K. Fukuda, Science **268**, 1466 (1995)

13. K. Nielsch, R. Wehrspohn, J. Barthel, J. Kirschner, U. Gösele, S. Fischer, H. Kronmüller, Appl. Phys. Lett. **79**, 1360 (2001)
14. A. Fert, L. Piraux, J. Magn. Magn. Mater. **200**, 338 (1999)
15. D.J. Sellmyer, M. Zheng, R. Skomski, J. Phys.: Condens. Matter **13**, R433 (2001)
16. P.M. Paulus, F. Luis, M. Kröll, G. Schmid, L.J. de Jongh, J. Magn. Magn. Mater. **224**, 180 (2001)
17. K. Nielsch et al., J. Magn. Magn. Mater. **249**, 234 (2002)
18. W. Schwarzacher, K. Attenborough, A. Michel, G. Nabiyouni, J.P. Meier, J. Magn. Magn. Mater. **165**, 23 (1997)
19. J. Lee et al., J. Appl. Phys. **91**, 8513 (2002)
20. A. Blondel, J.P. Meier, B. Doudin, J.Ph. Ansermet, Appl. Phys. Lett. **65**, 3019 (1994)
21. A. Radulescu, U. Ebels, Y. Henry, K. Ounadjela, J.L. Duvail, L. Piraux, IEEE Trans Magn. **36**, 3062 (2000)
22. T. Ohgai, X. Hoffer, L. Gravier, J.E. Wegrowe, J.P. Ansermet, Nanotechnology **14**, 978 (2003)
23. S. Dubois, J. Colin, J.L. Duvail, L. Piraux, Phys. Rev. B **61**, 14315 (2000)
24. J.M. García, A. Asenjo, M. Vázquez, P. Aranda, E. Ruiz-Hiztky, IEEE Trans. Magn. **36**, 2981 (2000)
25. G. Hadjipanayis et al., J. Appl. Phys. **91**, 6869 (2002)
26. T.G. Sorop, C. Untiedt, F. Luis, M. Kröll, M. Rasa, J. de Jongh, Phys. Rev. B **67**, 14402 (2003)
27. K. Nielsch, R. Hertel, R.B. Wehrspohn, J. Barthel, J. Kirschner, U. Gösele, S.F. Fischer, H. Kronmüller, IEEE Trans. Magn. **38**, 2571 (2002)
28. R. Hertel, in reference [13] p. 251; H. Forster et al., in reference [13] p. 181
29. M. Vázquez, D.-X. Chen, IEEE Trans. Magn. **31**, 1229 (1995)
30. M. Kröll et al., in reference [13] p. 241; J. Stankiewicz, F. Luis, A. Camón, M. Kröll, J. Bartolomé, W. Blau, J. Magn. Magn. Mater. (in press)
31. R. Skomski, H. Zeng, D.J. Sellmyer, in reference [13] p. 175
32. U. Ebels, A. Radulescu, Y. Henry, L. Piraux, K. Ounadjela, Phys. Rev. Lett. **84**, 983 (2000)
33. Y. Henry, A. Iovan, J.M. George, L. Piraux, Phys. Rev. B **66**, 184430 (2002)
34. A. Encinas-Oropesa, M. Demand, L. Piraux, I. Huynen, U. Ebels, Phys. Rev. B **63**, 104415 (2001); M. Demand et al., in reference [13] p. 228
35. U. Ebels, J.L. Duvail, P.E. Wigen, L. Piraux, L.D. Buda, K. Ounadjela, Phys. Rev. B **64**, 14421 (2001)
36. K. Nielsch, F. Müller, A.P. Li, U. Gösele, Adv. Mater. **12**, 342 (2000)
37. R.M. Metzger, V.V. Konovalov, M. Sum, T. Xu, G. Zangari, B. Xu, M. Benakli, W.D. Doyle, IEEE Trans. Magn. **36**, 1 (2000)
38. M. Hernández-Vélez, K. Pirota, F. Paszti, D. Navas, A. Climent, I. Schmytko, M. Vázquez (submitted)
39. K. Pirota, D. Navas, M. Hernández-Vélez, K. Nielsch, M. Vázquez, J. Alloys Comp. **369**, 18 (2004)
40. M. Vázquez, K. Nielsch, P. Vargas, J. Velázquez, D. Navas, K. Pirota, M. Hernández-Vélez, E. Vogel, J. Cartes, R.B. Wehrspohn, U. Gösele, Physica B **343**, 395 (2004)
41. R. Arias, D.L. Mills, Phys. Rev. B **67**, 94423 (2003)
42. Z.W. Wang et al., Phys. Rev. Lett. **89**, 27201 (2002)
43. C. Ramos, M. Vázquez, K. Nielsch, K. Pirota, J. Rivas, R.B. Wehrspohn, M. Tovar, R.D. Sánchez, U. Gösele, Proc. ICM'2003 (J. Magn. Magn. Mater. in press)
44. E.O. Samwel, P.R. Bissell, J.C. Lodder, J. Magn. Magn. Mater. **115**, 327 (1992)
45. J. Velázquez, M. Vázquez, IEEE Trans. Magn. **38**, 2477 (2002)
46. J. Velázquez, C. García, M. Vázquez, A. Hernando, Phys. Rev. B **54**, 9903 (1995)
47. J. Velázquez K. Pirota, M. Vázquez, IEEE Trans. Magn. **39**, 249 (2003)